Nano Research
2021, 14(3): 797–806

ISSN 1998-0124 CN 11-5974/O4
https://doi.org/10.1007/s12274-020-3116-y

Research Article

$LiYF_4$:Yb/$LiYF_4$ and $LiYF_4$:Yb,Er/$LiYF_4$ core/shell nanocrystals with luminescence decay times similar to YLF laser crystals and the upconversion quantum yield of the Yb,Er doped nanocrystals

Frederike Carl[1], Leonie Birk[1], Bettina Grauel[2], Monica Pons[2], Christian Würth[2], Ute Resch-Genger[2] (✉), and Markus Haase[1] (✉)

[1] *Institute of Chemistry of New Materials, Department Biology/Chemistry, University Osnabrueck, Barbarastr. 7, 49076 Osnabrueck, Germany*
[2] *Federal Institute for Materials Research and Testing (BAM), Division 1.2 Biophotonics, Richard-Willstaetter-Str. 11, 12489 Berlin, Germany*

Received: 18 June 2020 / **Revised:** 11 September 2020 / **Accepted:** 14 September 2020

ABSTRACT

We developed a procedure to prepare luminescent $LiYF_4$:Yb/$LiYF_4$ and $LiYF_4$:Yb,Er/$LiYF_4$ core/shell nanocrystals with a size of approximately 40 nm revealing luminescence decay times of the dopant ions that approach those of high-quality laser crystals of $LiYF_4$:Yb (Yb:YLF) and $LiYF_4$:Yb,Er (Yb,Er:YLF) with identical doping concentrations. As the luminescence decay times of Yb^{3+} and Er^{3+} are known to be very sensitive to the presence of quenchers, the long decay times of the core/shell nanocrystals indicate a very low number of defects in the core particles and at the core/shell interfaces. This improvement in the performance was achieved by introducing two important modifications in the commonly used oleic acid based synthesis. First, the shell was prepared via a newly developed method characterized by a very low nucleation rate for particles of pure $LiYF_4$ shell material. Second, anhydrous acetates were used as precursors and additional drying steps were applied to reduce the incorporation of OH^- in the crystal lattice, known to quench the emission of Yb^{3+} ions. Excitation power density (P)-dependent absolute measurements of the upconversion luminescence quantum yield (Φ_{UC}) of $LiYF_4$:Yb,Er/$LiYF_4$ core/shell particles reveal a maximum value of 1.25% at P of 180 W·cm^{-2}. Although lower than the values reported for $NaYF_4$:18%Yb,2%Er core/shell nanocrystals with comparable sizes, these Φ_{UC} values are the highest reported so far for $LiYF_4$:18%Yb,2%Er/$LiYF_4$ nanocrystals without additional dopants. Further improvements may nevertheless be possible by optimizing the dopant concentrations in the $LiYF_4$ nanocrystals.

KEYWORDS

nanocrystal, decay time, luminescence, $LiYF_4$, quantum yield, upconversion

1 Introduction

$LiYF_4$ and β-$NaYF_4$ are well-known host lattices for luminescent lanthanide ions owing to their large bandgap and low phonon frequencies, providing the necessary transparency for the luminescence of the dopant ions in the ultraviolet (UV), visible (vis) and near infrared (NIR) and minimizing internal luminescence quenching processes related to multiphonon relaxation (MPR) [1–9]. Growing large single crystals of high quality by the Czochralski process, however, is much easier for $LiYF_4$ than for β-$NaYF_4$ [2, 10–12]. In contrast to β-$NaYF_4$, Czochralski-grown crystals of lanthanide-doped $LiYF_4$ are commercially available from various suppliers and widely used as solid state laser materials. Well-known examples are $LiYF_4$:Pr [13–20], $LiYF_4$:Nd [21–29], $LiYF_4$:Yb [30–35], $LiYF_4$:Er [36–43], $LiYF_4$:Ho [44–50] and $LiYF_4$:Tm [51–56]. $LiYF_4$ laser crystals are grown under strict exclusion of water and humidity to avoid the incorporation of OH^- into the fluoride lattice which is a well-known luminescence quencher owing to its high-frequency vibrational modes [57, 58]. Laser crystals of $LiYF_4$:Er or $LiYF_4$:Tm are sometimes co-doped with Yb^{3+} ions, which enhances their absorption cross section in the NIR region and leads to energy transfer upconversion (ETU) emission of the crystals [59–61]. Lanthanide-doped $LiYF_4$ can also be prepared in the form of nanocrystals with very narrow size distribution [62–89]. This is usually done in high boiling oleic acid-based solvent mixtures, similar to the synthesis of $NaYF_4$ upconversion nanocrystals [62–66, 68–88]. Since the particles have a small size and display a relatively strong luminescence, they have been proposed for a variety of biomedical and bioimaging applications [79, 80, 83, 87], as well as for transparent displays [70, 74] and chemosensing [86]. Due to their large surface-to-volume ratio, however, surface quenching of the luminescence presents a severe problem, often reducing the photoluminescence quantum yield of the nanocrystals by several orders of magnitude compared to the bulk material. The standard method to solve this problem is to protect the surface of the nanometer-sized core particles with a shell of an inert material that blocks energy migration to the particle surface and effectively shields emissive lanthanide ions near the particle surface from quenchers in the surroundings. A common shell material is undoped $LiYF_4$, since energy migration in the particle core takes place via adjacent dopant ions [74]. Moreover, the lattice mismatch between an undoped $LiYF_4$ shell and the doped $LiYF_4$ core

Address correspondence to Markus Haase, markus.haase@uos.de; Ute Resch-Genger, ute.resch@bam.de

particle is low which reduces the risk of forming defect states at the core-shell interface. Other shell materials were nevertheless also investigated such as $LiGdF_4$ [65, 69], $LiLuF_4$ [71], $LiYbF_4$ [73], SiO_2 [63, 80], doped $LiYF_4$ [76, 77] as well as more complicated particle architectures involving multiple shells [69, 74].

In addition, the shell has to be sufficiently thick to reduce surface quenching of the luminescence as much as possible. Shell forming reactions with very low nucleation rates are therefore advantageous, since they reduce the loss of shell material due to the nucleation of new particles of pure shell material. Furthermore, not only the core-shell interface but also the core particle itself should contain only a negligible number of defects and impurity centers leading to luminescence quenching. Similar to laser crystals, the incorporation of OH^- into the fluoride host lattice must therefore be avoided during the synthesis.

The aim of this work was to develop a procedure for the preparation of $LiYF_4$:Yb/$LiYF_4$ core/shell particles with optical properties close to those of $LiYF_4$:Yb bulk crystals. This included measures to reduce the incorporation of OH^- into the crystal lattice of $LiYF_4$ as previously realized for $NaYF_4$:Yb,Er/$NaYF_4$ core/shell nanocrystals with high upconversion luminescence quantum yield [90]. Most challenging, however, was the search for a new shell forming reaction with the above mentioned properties, as the method used to form the shell of $NaYF_4$:Yb,Er/$NaYF_4$ core/shell nanocrystals cannot be applied to $LiYF_4$ nanoparticles.

After comparing the optical properties of the resulting core/shell particles with those of a high-quality laser crystal of $LiYF_4$:Yb, we prepared Yb,Er-doped particles and studied the upconversion quantum yield of $LiYF_4$:Yb,Er/$LiYF_4$ core/shell particles.

2 Experimental

2.1 Chemicals and materials

Anhydrous rare earth acetates were prepared as described previously [90]. Purified oleic acid was purchased from Fisher Scientific, 1-octadecene (technical grade, 90%) from Alfa Aesar, ammonium fluoride and lithium acetate from Sigma Aldrich. All materials were used as received.

2.2 Synthesis of $LiYF_4$:Yb(18%) and $LiYF_4$:Yb(18%), Er(2%) core particles

25 mL of oleic acid (HOA) and 25 mL 1-octadecene (ODE) were combined in a 250 mL three-neck round bottom flask and connected to a reflux condenser, heating mantle and temperature controller. The stirred solvent was degassed at 100 °C under vacuum (< 0.1 mbar, Schlenk-line) until the evolution of gas (water and air) came to an end. After cooling to room temperature using a water bath and switching to nitrogen flow, 0.6599 g (10 mmol) of anhydrous lithium acetate and 5 mmol of anhydrous rare earth acetates were added: 1.0642 g (4 mmol) of yttrium acetate, 0.3152 g (0.9) mmol of ytterbium acetate and 0.0344 g (0.1) mmol of erbium acetate in the case of $LiYF_4$:Yb(18%),Er(2%) particles or 1.0908 g (4.1 mmol) of yttrium acetate and 0.3152 g (0.9 mmol) of ytterbium acetate in the case of $LiYF_4$:Yb(18%) particles. The stirred mixture was again heated to 100 °C under vacuum and left at this temperature until the evolution of gas (acetic acid) ceased. The apparatus was refilled with nitrogen and the clear solution heated to 300 °C. Heating was stopped after 10 min and the mixture allowed to cool to 100 °C. To remove the acetic acid released during the heating step at 300 °C, vacuum was again applied and the solution degassed for one hour at 100 °C.

Subsequently, the apparatus was switched to nitrogen atmosphere and 0.9259 g (25 mmol) of dry NH_4F was added at 100 °C. To remove air, the vessel was subjected three times to a short vacuum (3–5 s) and refilled with nitrogen. The mixture was then heated to 300 °C and further stirred at this temperature and in nitrogen atmosphere for two hours. After cooling to room temperature, the cloudy, slightly yellowish solution was centrifuged. The yellow supernatant was decanted from the precipitate and controlled for dissolved particles by adding the equivalent amount of ethanol. In general, no precipitation was observed unless the heating time at 300 °C was reduced from 2 h to 30 min. In this special case, the solid was separated by centrifugation for further analysis and either dried or re-dispersed in hexane. The solid content of the reaction mixture obtained by decantation of the supernatant was combined with 10 mL of hexane and vigorously shaken to extract the core particles adhering to the LiF solid formed as by-product. After centrifugation, the core particles were precipitated by adding 10 mL of ethanol to the supernatant and separated by centrifugation. Subsequently, the particles were washed by redispersing the precipitate in hexane again, adding 10 mL of ethanol, and collecting the product by centrifugation. Colloidal solutions of the core particles were prepared by immediately re-dispersing some of this product in hexane. The remaining product was dried, yielding a matte white powder. Thermogravimetric analysis indicated a solid, non-volatile content of the dry powder of about 85 wt.%–90 wt.%, the remaining 10 wt.%–15 wt.% is attributed to the organic ligand shell of the particles.

2.3 Synthesis of core/shell particles with $LiYF_4$ shell

For the synthesis of core/shell particles, the core particles and the precursors for the $LiYF_4$ shell were combined in a molar ratio of 1:7. The shell is therefore expected to increase the volume of the core particles by a factor of 8 and their diameter by a factor of 2.

50 mL of HOA and 50 mL of ODE were combined in a 250 ml three-neck round bottom flask and connected to a reflux condenser, heating mantle and temperature controller. The stirred solvent was degassed at 100 °C under vacuum (< 0.1 mbar) at a Schlenk-line until the evolution of gas (water and air) stopped. After cooling to room temperature and switching to nitrogen flow, 4.6557 g (17.5 mmol) of anhydrous yttrium acetate was added. The stirred mixture was again heated to 100 °C under vacuum and left at this temperature until no more acetic acid was released. The apparatus was refilled with nitrogen and the clear solution heated to 300 °C. Heating was stopped after 10 min and the mixture was allowed to cool to 100 °C. To remove the acetic acid released during the heating step at 300 °C, vacuum was again applied and the solution was degassed at 100 °C until the evolution of gas (acetic acid) was finished.

In the meantime, 16.7 mL of HOA and 16.7 mL of ODE were combined in a second set-up consisting of a 250 mL three-neck round bottom flask, reflux condenser, heating mantle, and temperature controller. The stirred solvent was degassed at 100 °C under vacuum (< 0.1 mbar) at a Schlenk-line to remove water and oxygen. After cooling to room temperature and switching to nitrogen flow, 2.5 mmol of $LiYF_4$:Yb,(Er) core nanoparticles were added, taking into account the mass of the organic content of the particles. The stirred mixture was again heated to 100 °C under vacuum and left at this temperature

until no gas evolved from the solution.

The apparatus was refilled with nitrogen and the solution heated to 300 °C. Heating was stopped after reaching 300 °C and the mixture was allowed to cool to 100 °C. Vacuum was applied again and the solution degassed at 100 °C until no further gas evolved.

After switching to nitrogen atmosphere, 2.7237 g (105 mmol) LiF and the 100 °C hot solution of yttrium oleate were added to the solution of the $LiYF_4$:Yb,(Er) core particles at 100 °C. The solution was again degassed at 100 °C. After bubbling had stopped (max. 1 h), the apparatus was refilled with nitrogen and the solution heated to 300 °C. Heating was stopped after 6 h at 300 °C and the mixture was allowed to cool to room temperature overnight. Subsequently, the cloudy suspension was mixed with 300 mL HOA and 300 mL ODE to optimize the extraction of the particles and enhance their colloidal stability. The stirred suspension was degassed at 100 °C under vacuum (< 0.1 mbar) at a Schlenk-line until the evolution of gas (water and air) came to an end. The apparatus was refilled with nitrogen and the suspension heated to 300 °C. Heating was stopped after 10 min and the mixture allowed to cool to room temperature.

The cloudy suspension was centrifuged and treated as given above for the core particles, except that larger amounts of hexane and ethanol (40 mL each instead of 10 mL) were used for purification. In contrast to the synthesis of the core particles, most of the particles precipitated from the supernatant of the reaction mixture after the addition of ethanol. These particles were purified twice by precipitation with ethanol and by dissolving the precipitate in hexane.

For comparison, this core/shell synthesis procedure was also performed in the absence of core particles. In this case, the solution of the core particles was replaced by 33 mL of a deaerated 1:1 mixture of HOA and ODE. In contrast to the core/shell synthesis, the $LiYF_4$ product could not be extracted from the LiF by-product with hexane, because of the very large particle size. For the same reason, the precipitate obtained by centrifugation of the reaction mixture was directly investigated without heating the precipitate in 300 mL HOA and 300 mL ODE.

2.4 Particle characterization

Transmission electron microscopy (TEM) and powder X-ray diffraction (XRD) were used to determine the mean size, the size distribution [91], as well as the crystal phase and the phase purity of all particles [92, 93], respectively.

2.5 Single-crystal of $LiYF_4$:Yb(20%)

A Czochralski-grown laser crystal of high-quality $LiYF_4$:Yb(20%) was purchased from Optogama UAB, Lithuania. The disk-shaped crystal had a thickness of 2 mm and a diameter of 8 mm.

2.6 Absolute measurement of upconversion quantum yields at different excitation power densities

The quantum yields of the upconversion emission (Φ_{UC}) of the nanoparticle powders were determined absolutely at different excitation power densities (P) with a calibrated custom-designed integrating sphere setup previously reported [94]. The setup included a very stable 8 W 976 nm laser diode as excitation light source and two filter wheels with neutral density filters of known transmittance, both in the excitation channel for controlled attenuation of the excitation power density (P) in small steps. Another filter wheel with edge, band pass, and neutral density filters is placed in the detection channel to avoid detector saturation. Detection of the transmitted and emitted photons was done with a silicon CCD. The design and calibration of the setup, the beam profile characterization, and the measurement procedure were described in detail in a recent publication [94].

P-dependent Φ_{UC} were obtained from P-dependent upconversion luminescence (UCL) measurements by integration over all Er^{3+} emission bands between 370 and 890 nm. For the calculation of Φ_{UC}, see Eq. (1), the number of emitted photons (N_{em}) was obtained from blank and spectrally corrected UCL spectra. The number of absorbed photons (N_{abs}) was derived from transmission measurements of the sample and a non-emissive blank, as previously described [94]

$$\Phi_{UC}\,(P) = N_{em}/N_{abs}, \text{ for } \lambda_{em} < \lambda_{abs} \quad (1)$$

2.7 Time-resolved luminescence measurements

Luminescence decay kinetics were measured with an Edinburgh Instruments spectrofluorometer FLS-980 equipped with an electrically modulated 8 W 978 nm laser diode (40 μs long square pulse), a 100 mW 375 nm LED (5 μs long square pulses), and a red extended PMT (Hamamatsu R2658P). The decay curves were analyzed as previously reported [94].

3 Results and discussion

3.1 Core particle synthesis

HOA-based synthesis procedures for nanocrystalline $LiYF_4$ are usually based on the thermal decomposition of trifluoro acetates [63, 64, 66, 67, 78–89] or on the reaction of yttrium oleate with either ammonium fluoride and lithium oleate [77] or ammonium fluoride and lithium hydroxide [62, 65, 68–76]. Here, we prepared the $LiYF_4$ nanoparticles at temperatures above 200 °C via the reaction of ammonium fluoride with rare earth oleates and lithium oleate dissolved in oleic acid/octadecene [62, 65, 68–73, 74–77]. As usual, an excess of lithium oleate was used corresponding to twice the stoichiometric amount. For undoped $LiYF_4$ particles the formation reaction is thus given by

$$Y(OA)_3 + 2LiOA + 5NH_4F \rightarrow LiYF_4\text{-NPs} + LiF\downarrow + 5NH_3\uparrow + 5HOA$$

where OA, HOA and $LiYF_4$-NPs indicate oleate, oleic acid, and $LiYF_4$ nanoparticles, respectively.

After synthesis, the $LiYF_4$ particles adhere to the LiF by-product, which is separated from the reaction mixture by centrifugation.

If the reaction mixture was heated for a sufficiently long time, no particles could be precipitated from the supernatant by the addition of ethanol. Instead, the $LiYF_4$ particles were extracted from the LiF solid by washing with hexane.

We minimized the incorporation of UCL-quenching OH^- in the crystal lattice of the $LiYF_4$ particles by reducing the water content of the reaction mixture. Similar to our previous synthesis procedure for $NaYF_4$:Yb,Er/$NaYF_4$ core/shell upconversion particles with high Φ_{UC}, we used anhydrous rare earth acetates $RE(OAc)_3$ as precursors. In addition, high temperatures of up to 300 °C were applied for drying the solvent and releasing the acetic acid HOAc (see Experimental) [90]. Moreover, we avoided the use of LiOH or polar solvents like methanol and employed anhydrous lithium acetate LiOAc as lithium source. The solution of oleates required for the synthesis of the nanocrystals was thus formed by the reaction

$$RE(OAc)_3 + 2LiOAc + 5HOA \rightarrow RE(OA)_3 + 2LiOA + 5HOAc\uparrow$$

The above mentioned protocol was chosen because it yields

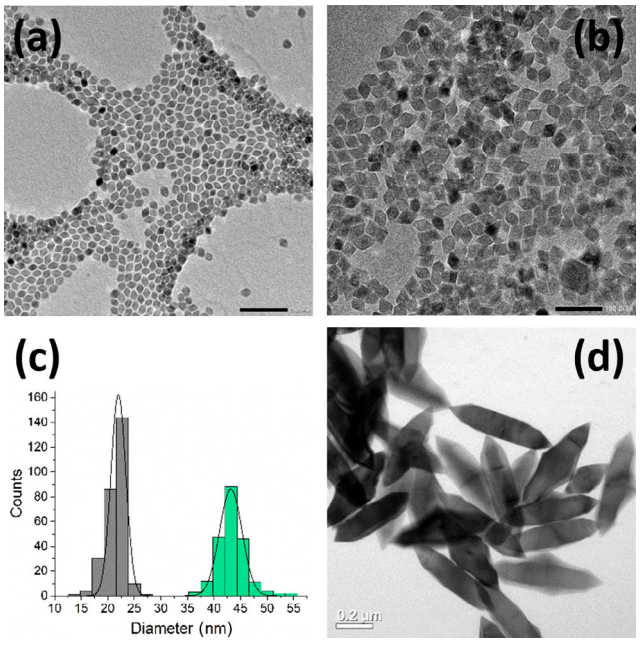

Figure 1 TEM images of (a) $LiYF_4$:Yb core and (b) $LiYF_4$:Yb/$LiYF_4$ core/shell particles. A molar ratio of core and shell material of 1 to 7 was used in the synthesis. (c) Size histograms of the long axis of the square bipyramidal particles shown in (a) and (b). The shell increases the mean particle size from 22 to 43 nm. (d) In the absence of core particles, the shell forming reaction yields very large $LiYF_4$ particles in the sub-μm size regime, proving that only a very small number of crystal seeds nucleate.

undoped and doped $LiYF_4$ particles with narrow size distribution and a mean size of approximately 20 nm. Core particles in this size range were found to yield $NaYF_4$:Yb,Er/$NaYF_4$ core/shell particles with the highest upconversion quantum yield [90]. The particles have the well-known square bipyramidal shape, as shown in Fig. 1(a) for Yb^{3+} doped $LiYF_4$ nanocrystals.

The small particle size indicates that a large number of $LiYF_4$ seeds are formed during the reaction. The reaction described above is therefore well suited to prepare a large number of $LiYF_4$ core particles with small size but not well suited to grow a $LiYF_4$ shell.

The latter requires a reaction where only a small number of crystal seeds nucleate, because otherwise the undesired formation of new particles of pure shell material competes with the formation of a shell on the core particles. Seeds of pure shell material are a particular problem when thick shells are required for complete passivation of the core, as, in this case, a large amount of shell precursor material has to be combined with only a small number of core particles. Despite these disadvantages, the above mentioned reactions are frequently used to synthesize both, the $LiYF_4$ particles as well as the $LiYF_4$ shell. To nevertheless minimize the nucleation of new $LiYF_4$ particles, the solution of the shell precursor is often added very slowly or in small portions to the solution of the core particles [78, 81, 88].

This time-consuming and complex procedure can be avoided by forming the shell via a reaction with a very low nucleation rate. We recently used this strategy by employing small α-Na_xYF_{3+x} particles with low x as shell precursor in the synthesis of β-$NaYF_4$:Yb,Er/$NaYF_4$ core/shell particles [90, 95]. Unfortunately, the same reaction cannot be used to form the shell of $LiYF_4$:Yb/$LiYF_4$ core/shell particles, since an analogue metastable phase does not exist in the $LiYF_4$ system.

3.2 The new shell forming reaction

We found, however, that a suitable shell-forming reaction is the reaction of solid lithium fluoride with a solution of yttrium oleate in oleic acid/octadecene

$$Y(OA)_3 + 4LiF \rightarrow LiYF_4 + 3LiOA$$

Similar to the reaction described above, the solution of yttrium oleate was prepared by dissolving anhydrous yttrium acetate in oleic acid/octadecene at high temperatures. In order to increase the reaction rate, we used $Y(OA)_3$ and LiF in a molar ratio of 1 to 6 instead of the stoichiometric ratio of 1 to 4.

When this reaction takes place in the presence of $LiYF_4$:Yb core particles, core/shell particles with narrow size distribution are obtained, as shown in Fig. 1(b) for a molar ratio of core and shell material of 1 to 7. The size histograms in Fig. 1(c) in fact show an increase in size from 22 nm of the core particles in Fig. 1(a) to 43 nm of the core/shell particles in Fig 1(b). This increase of the long axis of the square bipyramids corresponds to a shell thickness of about 5 nm, because the shell thickness d is connected to the apex angle α of the bipyramids of about 60° by $d = h \cdot \sin(\alpha/2)$ where h equals half the increase of the long axis (see Fig. S1 in the Electronic Supplementary Material (ESM) for details).

In the absence of core particles, however, the same reaction yields very large $LiYF_4$ particles with sizes exceeding 300 nm (Fig. 1(d)). The diffractograms in Fig. 2 confirm complete conversion to $LiYF_4$ after a reaction time of 6 h. The large particle size confirms that the shell reaction itself forms only a small number of crystal seeds.

The reaction is therefore not suitable for the synthesis of $LiYF_4$ nanoparticles with a small size, but very well suited to grow a shell on core particles which act as crystal seeds in the solution. The XRD data confirm that the core and the core/shell particles, as well as the large particles in Fig. 1(d), crystallize in

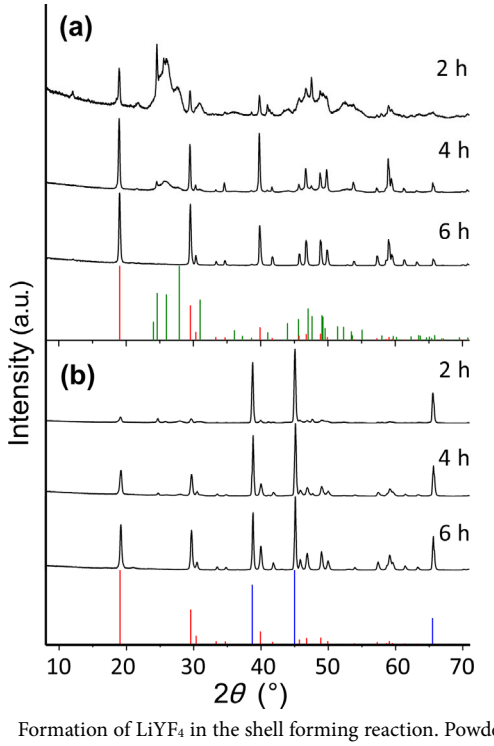

Figure 2 Formation of $LiYF_4$ in the shell forming reaction. Powder XRD of the materials obtained after different reaction times at 300 °C in the absence of core particles. (a) Small amount of solid precipitating from the supernatant of the reaction mixture after the addition of ethanol. (b) Solid content of the reaction mixture consisting of large $LiYF_4$ particles adhering to excess LiF. The reference data of $LiYF_4$ (PDF-No.: 01-081-2254), YF_3 (PDF-No.: 01-074-0911) and LiF (PDF-No.: 01-088-2298) given in red, green and blue, respectively, show that small YF_3 nanocrystals are the first product formed.

the tetragonal $LiYF_4$ phase (Fig. 2 and Fig. S2 in the ESM). A closer inspection of the materials formed at early stages of the synthesis reveals, however, that $LiYF_4$ is not the first product formed in either of the two procedures. Figure 2 displays the XRD data of the solids formed in the shell forming reaction in the absence of core particles. When this reaction is stopped already after 2 h at 300 °C, the solid in the reaction mixture consists almost entirely of LiF and only a very small amount of $LiYF_4$ particles (Fig. 2 (b)). A second solid can be precipitated in small amount from the supernatant of the reaction mixture by adding ethanol (Fig. 2 (a)). The XRD data show that this solid consists mainly of YF_3 and some $LiYF_4$ indicating that the following reaction took place (neglecting excess LiF)

$$Y(OA)_3 + (3+x)LiF \rightarrow (1-x)YF_3\text{-NPs} + xLiYF_4 + 3LiOA$$

Figure 2 shows that after two hours the value of x is very small, but with increasing reaction time the amount of YF_3 in the supernatant decreases while the amount of $LiYF_4$ increases in both, the supernatant and in the solid product produced. These results indicate that the YF_3 particles formed at the beginning of the reaction completely dissolve at later stages of the synthesis ($x \rightarrow 1$) and yield $LiYF_4$ particles that partly adhere to the excess of solid LiF. It is not yet clear whether nucleation of the $LiYF_4$ seeds takes place heterogeneously on the surface of the LiF solid or homogeneously in solution, followed by adhesion of the seeds to the LiF solid.

The first product formed in the synthesis of the doped $LiYF_4$ core particles seems to be also lanthanide trifluoride. When the core particle synthesis is stopped after 30 min rather than after 2 h, a white powder precipitates when ethanol is added to the supernatant of the reaction mixture. The XRD data indicate that the solid consists of very small oleate capped doped YF_3 particles (Fig. S3 in the ESM). After 2 h of reaction at 300 °C, no solid can be precipitated any more from the supernatant, and extraction of the LiF solid yields nothing but the doped $LiYF_4$ particles shown in Fig. 1 (see also the XRD data in Fig. S2 in the ESM). This indicates that small doped YF_3 particles are formed intermediately in the synthesis of the core particles

$$Y(OA)_3 + 2LiOA + 5NH_4F \rightarrow (1-x)YF_3\text{-NPs} + xLiYF_4\text{-NPs} + (2-x)LiF\downarrow + 5NH_3\uparrow + 5HOA$$

Similar to the shell forming reaction, the small particles dissolve at later stages of the synthesis ($x \rightarrow 1$) leading to doped $LiYF_4$ particles that adhere to the LiF by-product.

3.3 Comparison of the optical properties with an Yb:YLF laser crystal

To confirm the passivation of the $LiYF_4$:Yb core particles by the inert $LiYF_4$ shell, we determined the luminescence decay kinetics of the Yb^{3+} dopant known to sensitively respond to environmental effects and the presence of quenchers [96, 97]. Since our particles contain a high concentration of Yb^{3+}, rapid energy migration occurs via adjacent Yb^{3+} ions. In the absence of a $LiYF_4$ shell, this leads to efficient luminescence quenching at the particle surface. Even in the presence of a $LiYF_4$ shell, however, quenching can occur at the core/shell interface or at defects in the crystal lattice. The lifetime of the excited Yb^{3+} state is therefore a good indicator of the quality of the core/shell particle. Figure 3 displays the Yb^{3+} decay curves of our core and core/shell particles containing 18% Yb^{3+} in the core.

For comparison, also the Yb^{3+} decay curve of a commercial high-quality $LiYF_4$:Yb(20%) laser crystal was measured which had a size of several millimeters and was grown by the Czochralski process.

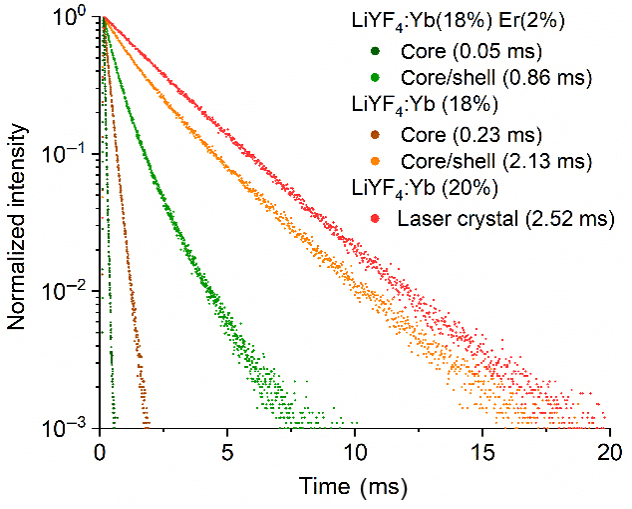

Figure 3 Luminescence decay of the Yb^{3+} emission of powders of mono-doped $LiYF_4$:Yb and co-doped $LiYF_4$:Yb,Er core and core/shell particles and of a $LiYF_4$:Yb laser crystal. The fastest decay is observed for $LiYF_4$:Yb and $LiYF_4$:Yb,Er core particles due to severe surface quenching. The Yb^{3+} luminescence of the corresponding core/shell particles decays significantly slower than the emission of the core particles. Due to energy transfer from Yb^{3+} to Er^{3+}, the emission of the Yb,Er-doped core and core/shell particles decays faster than the emission of the corresponding Yb-doped particles lacking the activator Er^{3+}. The decay of the $LiYF_4$:Yb core/shell particles is already very similar to the slow decay of the laser crystal.

The decay times given in the figure are intensity-weighted average lifetimes derived from multiexponential fits of the luminescence decay profiles. Remarkably, the decay time of the $LiYF_4$:Yb(18%)/$LiYF_4$ core/shell particles of 2.1 ms is almost identical to the decay time of the laser crystal: The laser crystal shows a lifetime of the Yb^{3+} emission of approximately 2.5 ms, in agreement with the specification given by the supplier of the crystal (2.1 ms).

In the absence of surface passivation, a much faster decay time of Yb^{3+} of 230 μs is observed showing that the $LiYF_4$ shell increases the Yb^{3+} luminescence lifetime by a factor of 9.3. These results indicate that our improved synthesis method not only leads to a very efficient passivation by the shell but also to a low defect concentration in the particle cores and at the core/shell interface. This leads to core/shell particles with optical properties very similar to those of the bulk material.

3.4 Yb,Er doped $LiYF_4$ core and core/shell nanocrystals

Next, we used our newly developed method to prepare upconverting nanocrystals with core particles doped with Yb^{3+} and Er^{3+}. The TEM images in the upper part of Fig. 4 indicate that co-doping with 2% Er has only a weak influence on the reactions, as the particle size of the core and the core/shell particles are similar to those shown in Fig. 1. This is further confirmed by the particle size histograms and the XRD data displayed in Figs. S4 and S2 in the ESM, respectively.

Figure 3 also includes the decay kinetics of the Yb^{3+} emission of our co-doped systems, the $LiYF_4$:Yb,Er core and core/shell nanoparticles. The figure shows that co-doping of the particle cores with 2% of Er^{3+} decreases the lifetime of the excited Yb^{3+} ions in both, the core as well as the core/shell particles. This was to be expected, since energy transfer from Yb^{3+} to Er^{3+} ions is known to occur in $LiYF_4$:Yb,Er crystals [59, 60]. This energy transfer results in upconversion emission of the co-doped particles, as shown in Fig. 4. Compared to the upconversion emission spectrum of the microcrystalline β-$NaYF_4$:Yb,Er

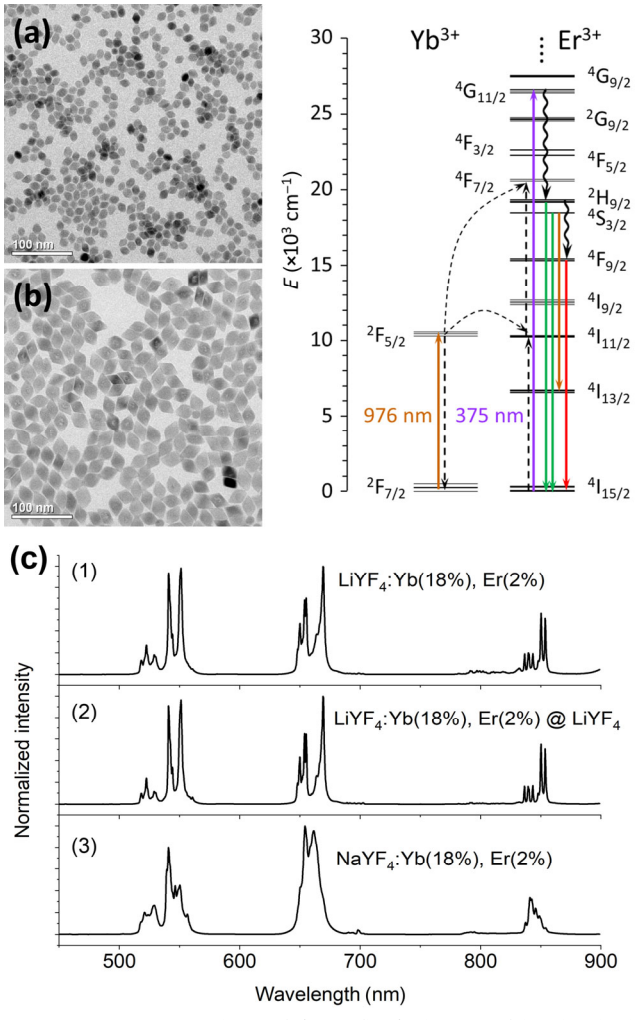

Figure 4 TEM images (upper left panel) of (a) $LiYF_4$:Yb(18%),Er(2%) core particles and (b) $LiYF_4$:Yb(18%),Er(2%)/$LiYF_4$ core/shell particles. Energy level diagram (upper right panel) of Yb^{3+} and Er^{3+} with crystal field splitting of the levels in $LiYF_4$ [98, 99]. The arrows indicate direct excitation of Er^{3+} at 375 nm and UC excitation at 976 nm and the main Er^{3+} emission bands in the green, red, and NIR spectral region (~ 850 nm). (c) Normalized luminescence spectra (lower panel) of the upconversion emission of (1) 18 nm $LiYF_4$:Yb(18%),Er(2%) core particles, (2) the corresponding $LiYF_4$:Yb(18%),Er(2%)/$LiYF_4$ core/shell particles, and, for comparison, (3) a microcrystalline $NaYF_4$:Yb(18%),Er(2%) upconversion phosphor. The latter displays a different crystal field splitting of the emission lines due to the different point symmetry of the rare-earth lattice sites compared to $LiYF_4$:Yb,Er. All spectra were recorded with the same spectral resolution.

upconversion phosphor (Fig. 4), the crystal field splitting of the Er^{3+} emission lines in the luminescence spectrum of $LiYF_4$:Yb,Er is different, since the point symmetry of the rare earth sites in the inverse scheelite ($CaWO_4$) structure of $LiYF_4$ is S_4 rather than C_{3h} [1, 2, 100, 101].

The decay kinetics of the green and red Er^{3+} emission of the co-doped core/shell particles are displayed in Fig. 5. The figure clearly shows that direct excitation of the Er^{3+} ions at 375 nm results in shorter decay times than excitation at 978 nm. This was to be expected, as excitation at 978 nm mainly excites the Yb^{3+} ions which show a comparatively long lifetime of about 0.86 ms even in the presence of Er^{3+} (Fig. 3). Since energy transfer from Yb^{3+} to Er^{3+} persists as long as the number of excited Yb^{3+} ions is sufficiently high, excitation of Er^{3+} via the ETU mechanism results in a longer decay time of the red and green Er^{3+} emission than short-pulsed direct excitation at 375 nm.

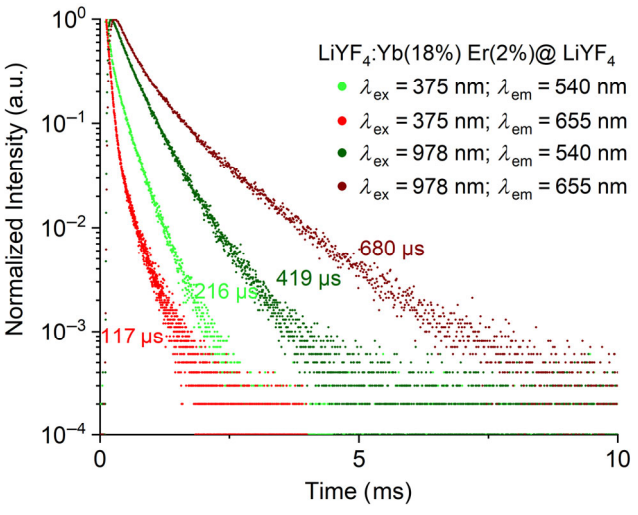

Figure 5 Luminescence decays of the red and green emission bands of $LiYF_4$:Yb^{3+},Er^{3+}/$LiYF_4$ core/shell particles for 375 and 978 nm excitation.

The decay times given in Fig. 5 are again intensity-weighted average lifetimes derived from multiexponential fits of the luminescence decay profiles. This method yields very low residuals in all cases. However, to be able to compare the luminescence kinetics of our core/shell particles with literature data reported for a single crystal of $LiYF_4$:Yb,Er, we fitted our decay profiles also with a double exponential tail fit. Both methods yield fits of comparable quality.

The results of the double exponential fits are summarized in Table 1, together with the data reported for the single crystal. When the Er^{3+} ions are excited directly, the decay times of the red and green Er^{3+} emission of the core/shell particles are even slightly longer than those of the single crystal. This result, together with the close match between the Yb^{3+} lifetimes of the core/shell particles and the Yb^{3+} laser crystal (see Fig. 3), shows again that our $LiYF_4$ shell protects the dopant ions in the core particles very well.

Table 1 Comparison of the double exponential decay fits of the green and red Er^{3+} emission of our $LiYF_4$:18%Yb,2%Er/$LiYF_4$ core/shell particles and a single crystal of $LiYF_4$:18%Yb,2%Er [102]

Direct excitation of Er^{3+}					
	$\lambda_{exc.}$ (nm)	$\lambda_{em.}$ (nm)	τ_1 (µs)	τ_2 (µs)	
Core/shell nanocrystals	375	540	91	315	Green
Single crystal Ref. [102]	363	550	48	211	
Core/shell nanocrystals	375	655	66	295	Red
Single crystal Ref. [102]	363	667	79	—	
Excitation of Er^{3+} via Yb^{3+}					
	$\lambda_{exc.}$ (nm)	$\lambda_{em.}$ (nm)	τ_1 (µs)	τ_2 (µs)	
Core/shell nanocrystals	978	540	295	602	Green
Single crystal Ref. [102]	971	550	412	982	
Core/shell nanocrystals	978	655	353	1,099	Red
Single crystal Ref. [102]	971	667	260	1,066	

When the materials are excited in the NIR, involving light absorption by Yb^{3+} and subsequent energy transfer to the emissive Er^{3+} ions, the red emission bands of the core/shell particles and the single crystal show very similar decay times, whereas the green emission of the nanocrystals decays slightly faster. The latter indicates that the energy transfer processes are not identical in both materials. The reason could be a different distribution of the Er^{3+} ions in the core/shell particles and the single crystal, which could possibly favor cross-relaxation in the former known to decrease the lifetime of the green emitting $^2S_{3/2}$ state of Er^{3+} in $LiYF_4$ [102]. A detailed analysis of the distribution of dopant ions, however, is currently beyond reach.

3.5 Absolute measurement of the upconversion quantum yields

Figure 6 displays absolute measurements of the *P*-dependent upconversion quantum yields (Φ_{UC}) of the Yb,Er doped samples. As highlighted in Fig. 6, the inert $LiYF_4$ shell significantly increases Φ_{UC}, the enhancement factor depending on *P*. The largest enhancement of more than a factor of 100 is observed at low *P* and decreases at higher *P*. A maximum Φ_{UC} value of 1.25% is determined at 180 W·cm^{-2} for the core/shell particles with the 5 nm $LiYF_4$ shell. This is almost one order of magnitude lower than the maximum Φ_{UC} of the microcrystalline β-$NaYF_4$:Yb,Er upconversion phosphor. A lower quantum yield is, however, to be expected, as bulk β-$NaYF_4$:Yb,Er is reported to be the most efficient upconversion material known today.

The reason for the higher quantum yield of β-$NaYF_4$:Yb,Er compared to $LiYF_4$:Yb,Er could be the multisite formation (disordered structure) known to occur in the β-$NaYF_4$ host lattice, resulting in ideal resonance conditions for the Yb-to-Er energy transfer in this material [1].

Our Φ_{UC} values are the highest reported so far for $LiYF_4$:18%Yb,2%Er nanocrystals of small size. For example, X. Xue et al. determined Φ_{UC} values of about 0.3% and 0.4% for nanoparticles without shell and sizes of 30 and 100 nm, respectively [72]. Φ_{UC} measurements of relatively large diamond-shaped $LiYF_4$:20%Yb,2%Er/$LiYF_4$ core/shell nanocrystals (length about 200 nm, width ≥ 70 nm) in cyclohexane revealed a value of 1.05% [78]. Significantly higher Φ_{UC} values of 2.28% and 5.7% (P = 6.2 W·cm^{-2}) have been reported, however, for Cd^{2+} co-doped $LiYF_4$:20%Yb,2%Er,10%Cd/$LiYF_4$ core/shell nanocrystals and for single crystals of $LiYF_4$ doped with only 2% Yb^{3+} and 1% Er^{3+}, respectively [78, 103]. The latter can indicate a different optimum doping concentration for $LiYF_4$ crystals compared to ß-$NaYF_4$, which was also observed for SrF_2 single crystals [104]. Methods for increasing multisite formation in $LiYF_4$ nanocrystals and a systematic search for optimal dopant concentrations may therefore be useful strategies to further increase Φ_{UC} of $LiYF_4$:Yb,Er nanocrystals.

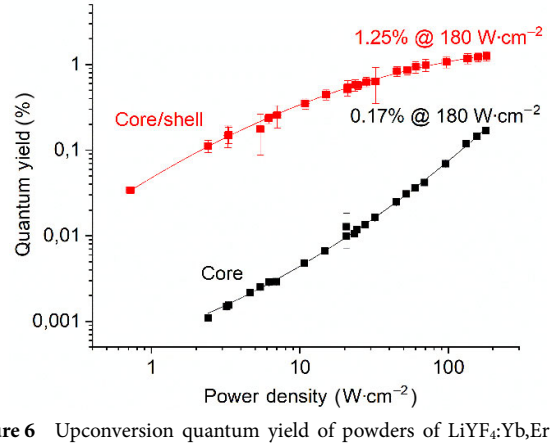

Figure 6 Upconversion quantum yield of powders of $LiYF_4$:Yb,Er core and core/shell particles as function of excitation power density *P*. The quantum yield of the 18 nm $LiYF_4$:Yb(18%),Er(2%) core particles is one to two orders of magnitude lower than the quantum yield of the corresponding $LiYF_4$:Yb(18%),Er(2%)/$LiYF_4$ core/shell particles.

4 Conclusion and outlook

In conclusion, we prepared $LiYF_4$:Yb/$LiYF_4$ core/shell nanocrystals displaying a decay time of the Yb^{3+} emission very similar to Czochralski-grown laser crystals of $LiYF_4$:Yb. Core/shell particles co-doped with Er^{3+} show similar decay kinetics of the red and green emission band as single crystals of $LiYF_4$ containing the same dopant concentrations. These results confirm the high quality of our core/shell synthesis procedure. The long lifetimes of the excited dopant ions indicate a very low defect density in the core/shell particles and an efficient shielding of the approximately 20 nm large particle cores by the inert shell of approximately 5 nm thickness. This was achieved by introducing two important modifications into the previously used synthetic route: We developed a new method to prepare the $LiYF_4$ shell, which is based on a reaction with a very low tendency to form separate new particles of pure shell material. This not only ensures that the vast majority of the shell precursor reacts with the core particles, but also that the shell can be prepared via a simple heating-up method without the necessity of slowly adding a precursor solution. By using anhydrous rare earth acetates and anhydrous lithium acetate for the synthesis and drying the oleic acid/octadecene solvent at higher temperatures, we could reduce the probability of incorporating OH^- into the fluoride lattice as previously reported for the synthesis of highly luminescent $NaYF_4$:Yb,Er/$NaYF_4$ core/shell nanocrystals [90]. Co-doping the core particles with Er^{3+} leads to energy transfer from Yb^{3+} to Er^{3+} resulting in upconversion emission. Absolute measurements of the excitation power density (*P*)-dependent upconversion quantum yield (Φ_{UC}) show the highest values reported so far for $LiYF_4$:18%Yb,2%Er/$LiYF_4$ core/shell nanocrystals of small size and without additional dopants. However, despite the efficient surface shielding confirmed by time-resolved luminescence measurements, the values are approximately one order of magnitude lower compared to the quantum yield of microcrystalline $NaYF_4$:Yb,Er upconversion phosphor powder.

We assume that $LiYF_4$ lacks the disordered structure of β-$NaYF_4$, which is believed to be the main reason for the high upconversion efficiency of β-$NaYF_4$. Furthermore, the optimum dopant concentrations could be different for the two hosts.

Acknowledgements

We thank the German Science Foundation DFG for financial support (grants RE 1203/18-1 and HA 1649/7-1).

Funding note: Open Access funding enabled and organized by Projekt DEAL.

Electronic Supplementary Material: Supplementary material (calculated shell thickness, X-ray diffraction measurements, TEM measurement of small YF_3 particles, size histograms of the Yb,Er doped $LiYF_4$ core and core/shell particles) is available in the online version of this article at https://doi.org/10.1007/s12274-020-3116-y.

References

[1] Renero-Lecuna, C.; Martín-Rodríguez, R.; Valiente, R.; González, J.; Rodríguez, F.; Krämer, K. W.; Güdel, H. U. Origin of the high upconversion green luminescence efficiency in β-$NaYF_4$:2%Er^{3+}, 20%Yb^{3+}. *Chem. Mater.* **2011**, *23*, 3442–3448.

[2] Lage, M. M.; Moreira, R. L.; Matinaga, F. M.; Gesland, J. Y. Raman and infrared reflectivity determination of phonon modes and crystal structure of czochralski-grown $NaLnF_4$ (Ln = La, Ce, Pr, Sm, Eu, and Gd) single crystals. *Chem. Mater.* **2005**, *17*, 4523–4529.

[3] Miller, S. A.; Rast, H. E.; Caspers, H. H. Lattice vibrations of $LiYF_4$. *J. Chem. Phys.* **1970**, *52*, 4172–4175.

[4] Salaün, S.; Fornoni, M. T.; Bulou, A.; Rousseau, M.; Simon, P. and Gesland, J. Y. Lattice dynamics of fluoride scheelites: I. Raman and infrared study of $LiYF_4$ and $LiLnF_4$ (Ln = Ho, Er, Tm and Yb). *J. Phys.: Condens. Matter* **1997**, *9*, 6941–6956.

[5] Schultheiss, E.; Scharmann, A.; Schwabe, D. Lattice vibrations in $BiLiF_4$ and $YLiF_4$. *Phys. Stat. Sol. (B)* **1986**, *138*, 465–475.

[6] Sarantopoulou, E.; Raptis, Y. S.; Zouboulis, E.; Raptis, C. Pressure and temperature-dependent Raman study of $YLiF_4$. *Phys. Rev. B* **1999**, *59*, 4154–4162.

[7] Zhang, X. X.; Schulte, A.; Chai, B. H. T. Raman spectroscopic evidence for isomorphous structure of $GdLiF_4$ and $YLiF_4$ laser crystals. *Solid State Commun.* **1994**, *89*, 181–184.

[8] Salaün, S.; Bulou, A.; Rousseau, M.; Hennion, B.; Gesland, J. Y. Lattice dynamics of fluoride scheelites: II. Inelastic neutron scattering in $LiYF_4$ and modelization. *J. Phys.: Condens. Matter* **1997**, *9*, 6957–6968.

[9] Minisini, B.; Wang, Q. A.; Tsobnang, F. *Ab initio* investigation of the lattice dynamics of fluoride scheelite $LiYF_4$. *J. Phys.: Condens. Matter* **2005**, *17*, 4953–4962.

[10] Kaminskii, A. A. *Laser Crystals*; Springer: Berlin, 1990.

[11] Thoma, R. E.; Hebert, G. M.; Insley, H.; Weaver, C. F. Phase equilibria in the system sodium fluoride-yttrium fluoride. *Inorg. Chem.* **1963**, *2*, 1005–1012.

[12] Thoma, R. E.; Insley, H.; Hebert, G. M. The sodium fluoride-lanthanide trifluoride systems. *Inorg. Chem.* **1966**, *5*, 1222–1229.

[13] Metz, P. W.; Reichert, F.; Moglia, F.; Müller, S.; Marzahl, D. T.; Kränkel, C.; Huber, G. High-power red, orange, and green Pr^{3+}:$LiYF_4$ lasers. *Opt. Lett.* **2014**, *39*, 3193–3196.

[14] Sandrock, T.; Danger, T.; Heumann, E.; Huber, G.; Chai, B. H. T. Efficient continuous wave-laser emission of Pr^{3+}-doped fluorides at room temperature. *Appl. Phys. B* **1994**, *58*, 149–151.

[15] Qu, B.; Xu, B.; Cheng, Y.; Luo, S.; Xu, H.; Bu, Y.; Camy, P.; Doualan, J. L.; Moncorge, R.; Cai, Z. InGaN-LD-pumped Pr^{3+}:$LiYF_4$ continuous-wave laser at 915 nm. *IEEE Photonics J.* **2014**, *6*, 1–11.

[16] Cai, Z. P.; Qu, B.; Cheng, Y. J.; Luo, S. Y.; Xu, B.; Xu, H. Y.; Luo, Z. Q.; Camy, P.; Doualan, J. L.; Moncorgé, R. Emission properties and CW laser operation of Pr:YLF in the 910 nm spectral range. *Optics Express* **2014**, *22*, 31722–31728.

[17] Qu, B.; Moncorgé, R.; Cai, Z. P.; Doualan, J. L.; Xu, B.; Xu, H. Y.; Braud, A.; Camy, P. Broadband-tunable CW laser operation of Pr^{3+}:$LiYF_4$ around 900 nm. *Opt. Lett.* **2015**, *40*, 3053–3056.

[18] Luo, S. Y.; Cai, Z. P.; Xu, H. Y.; Liu, X. F.; Chen, H.; Cao, Y.; Li, L. Diode-pumped 915-nm Pr:YLF laser passively mode-locked with a SESAM. *Opt. Express* **2018**, *26*, 24695–24701.

[19] Luo, S. Y.; Xu, B.; Xu, H. Y.; Cai, Z. P. High-power self-mode-locked Pr:YLF visible lasers. *Appl. Opt.* **2017**, *56*, 9552–9555.

[20] Tanaka, H.; Fujita, S.; Kannari, F. High-power visibly emitting Pr^{3+}:YLF laser end pumped by single-emitter or fiber-coupled GaN blue laser diodes. *Appl. Opt.* **2018**, *57*, 5923–5928.

[21] Huang, Y. J.; Tzeng, Y. S.; Tang, C. Y.; Huang, Y. P.; Chen, Y. F. Tunable GHz pulse repetition rate operation in high-power TEM_{00}-mode Nd:YLF lasers at 1,047 nm and 1,053 nm with self mode locking. *Opt. Express* **2012**, *20*, 18230–18237.

[22] Hardman, P. J.; Clarkson, W. A.; Friel, G. J.; Pollnau, M.; Hanna, D. C. Energy-transfer upconversion and thermal lensing in high-power end-pumped Nd:YLF laser crystals. *IEEE J. Quant. Electron.* **1999**, *35*, 647–655.

[23] Liang, H. C.; Wu, C. S. Diode-pumped orthogonally polarized self-mode-locked Nd:YLF lasers subject to gain competition and thermal lensing effect. *Opt. Express* **2017**, *25*, 13697–13704.

[24] Weingarten, K. J.; Shannon, D. C.; Wallace, R. W.; Keller, U. Two-gigahertz repetition-rate, diode-pumped, mode-locked Nd:YLF laser. *Opt. Lett.* **1990**, *15*, 962–964.

[25] Malcolm, G. P. A.; Curley, P. F.; Ferguson, A. I. Additive-pulse mode locking of a diode-pumped Nd:YLF laser. *Opt. Lett.* **1990**, *15*, 1303–1305.

[26] Juhasz, T.; Lai, S. T.; Pessot, M. A. Efficient short-pulse generation from a diode-pumped Nd:YLF laser with a piezoelectrically induced diffraction modulator. *Opt. Lett.* **1990**, *15*, 1458–1460.

[27] Weingarten, K. J.; Keller, U.; Chiu, T. H.; Ferguson, J. F. Passively mode-locked diode-pumped solid-state lasers that use an antiresonant Fabry-Perot saturable absorber. *Opt. Lett.* **1993**, *18*, 640–642.

[28] Danailov, M. B.; Cerullo, G.; Magni, V.; Segala, D.; De Silvestri, S. Nonlinear mirror mode locking of a cw Nd:YLF laser. *Opt. Lett.* **1994**, *19*, 792–794.

[29] Huang, Y. J.; Tang, C. Y.; Lee, W. L.; Huang, Y. P.; Huang, S. C.; Chen, Y. F. Efficient passively Q-switched Nd:YLF TEM_{00}-mode laser at 1,053 nm: Selection of polarization with birefringence. *Appl. Phys. B* **2012**, *108*, 313–317.

[30] Kawanaka, J.; Yamakawa, K.; Nishioka, H.; Ueda, K. I. Improved high-field laser characteristics of a diode-pumped Yb:$LiYF_4$ crystal at low temperature. *Opt. Express* **2002**, *10*, 455–460.

[31] Zapata, L. E.; Ripin, D. J.; Fan, T. Y. Power scaling of cryogenic Yb:$LiYF_4$ lasers. *Opt. Lett.* **2010**, *35*, 1854–1856.

[32] Miller, D. E.; Ochoa, J. R.; Fan, T. Y. Cryogenically cooled, 149 W, Q-switched, Yb:$LiYF_4$ laser. *Opt. Lett.* **2013**, *38*, 4260–4261.

[33] Kawanaka, J.; Nishioka, H.; Inoue, N.; Ueda, K. I. Tunable continuous-wave Yb:YLF laser operation with a diode-pumped chirped-pulse amplification system. *Appl. Opt.* **2001**, *40*, 3542–3546.

[34] Fan, T. Y.; Ripin, D. J.; Aggarwal, R. L.; Ochoa, J. R.; Chann, B.; Tilleman, M.; Spitzberg, J. Cryogenic Yb^{3+}-doped solid-state lasers. *IEEE J. Select. Top. Quant. Electron.* **2007**, *13*, 448–459.

[35] Ter-Gabrielan, N.; Fromzel, V.; Sanamyan, T.; Dubinskii, M. Highly-efficient Q-switched Yb:YLF laser at 995 nm with a second harmonic conversion. *Opt. Mater. Express* **2017**, *7*, 2396–2403.

[36] Kintz, G. J.; Allen, R.; Esterowitz, L. cw and pulsed 2.8 μm laser emission from diode-pumped Er^{3+}:$LiYF_4$ at room temperature. *Appl. Phys. Lett.* **1987**, *50*, 1553–1555.

[37] Kintz, G. J.; Esterowitz, L.; Rosenblatt, G.; Stoneman, R. Diode pumped cw 2.8 Pm Er-$LiYF_4$ laser with high slope efficiency. In *Proceedings of Conference Proceedings LEOS Lasers and Electro-Optics Society*, Santa Clara, USA, 1988, pp 327–329.

[38] Auzel, F.; Hubert, S.; Meichenin, D. Multifrequency room-temperature continuous diode and Ar* laser-pumped Er^{3+} laser emission between 2.66 and 2.85 μm. *Appl. Phys. Lett.* **1989**, *54*, 681–683.

[39] Messner, M.; Heinrich, A.; Unterrainer, K. High-energy diode side-pumped Er:$LiYF_4$ laser. *Appl. Opt.* **2018**, *57*, 1497–1503.

[40] Wetter, N. U.; Deana, A. M.; Ranieri, I. M.; Gomes, L.; Baldochi, S. L. Influence of excited-state-energy upconversion on pulse shape in quasi-continuous-wave diode-pumped Er:$LiYF_4$ Lasers. *IEEE J. Quant. Electron.* **2010**, *46*, 99–104.

[41] Dergachev, A.; Moulton, P. F. Tunable CW Er:YLF diode-pumped

laser. In *Proceedings of Advanced Solid-State Photonics*, San Antonio, Texas United States, 2003, paper 3.
[42] Jensen, T.; Diening, A.; Huber, G.; Chai, B. H. T. Investigation of diode-pumped 2.8-μm Er:$LiYF_4$ lasers with various doping levels. *Opt. Lett.* **1996**, *21*, 585–587.
[43] Hong, J. Q.; Zhang, L. H.; Xu, M.; Hang, Y. Effect of erbium concentration on optical properties of Er:YLF laser crystals. *Infrared Phys. Technol.* **2017**, *80*, 38–43.
[44] Aggarwal, R. L.; Ripin, D. J.; Ochoa, J. R.; Fan, T. Y. Measurement of thermo-optic properties of $Y_3Al_5O_{12}$, $Lu_3Al_5O_{12}$, $YAlO_3$, $LiYF_4$, $LiLuF_4$, BaY_2F_8, $KGd(WO_4)_2$, and $KY(WO_4)_2$ laser crystals in the 80–300 K temperature range. *J. Appl. Phys.* **2005**, *98*, 103514.
[45] Fonnum, H.; Lippert, E.; Haakestad, M. W. 550 mJ Q-switched cryogenic Ho:YLF oscillator pumped with a 100 W Tm:fiber laser. *Opt. Lett.* **2013**, *38*, 1884–1886.
[46] Schellhorn, M. A comparison of resonantly pumped Ho:YLF and Ho:LLF lasers in CW and Q-switched operation under identical pump conditions. *Appl. Phys. B* **2011**, *103*, 777–788.
[47] Koen, W.; Bollig, C.; Strauss, H.; Schellhorn, M.; Jacobs, C.; Esser, M. J. D. Compact fibre-laser-pumped Ho:YLF oscillator–amplifier system. *Appl. Phys. B* **2010**, *99*, 101–106.
[48] Kwiatkowski, J.; Jabczynski, J. K.; Zendzian, W. An efficient continuous-wave and Q-switched single-pass two-stage Ho:YLF MOPA system. *Opt. Laser Technol.* **2015**, *67*, 93–97.
[49] Kwiatkowski, J. Highly efficient high power CW and Q-switched Ho:YLF laser. *Opto-Electron. Rev.* **2015**, *23*, 165–171.
[50] Coluccelli, N.; Lagatsky, A.; Di Lieto, A.; Tonelli, M.; Galzerano, G.; Sibbett, W.; Laporta, P. Passive mode locking of an in-band-pumped Ho:$YLiF_4$ laser at 2.06 μm. *Opt. Lett.* **2011**, *36*, 3209–3211.
[51] Ding, Y.; Zhang, D. X.; Wang, W.; Yao, B. Q.; Duan, X. M.; Ju, Y. L.; Wang, Y. Z. High power Tm:YLF laser operating at 1.94 μm. *Optik* **2015**, *126*, 855–857.
[52] Zhang, B.; Li, L.; He, C. J.; Tian, F. J.; Yang, X. T.; Cui, J. H.; Zhang, J. Z.; Sun, W. M. Compact self-Q-switched Tm:YLF laser at 1.91 μm. *Opt. Laser Technol.* **2018**, *100*, 103–108.
[53] Gorajek, Ł.; Jabczyński, J. K.; Żendzian, W.; Kwiatkowski, J.; Jelinkova, H.; Sulc, J.; Nemec, M. High repetition rate, tunable, Q-switched diode pumped Tm:YLF laser. *Opto-Electron. Rev.* **2009**, *17*, 309–317.
[54] Pomeranz, L. A.; Budni, P. A.; Lemons, M. L.; Miller, C. A.; Mosto, J. R.; Pollak, T. M. and Chicklis, E. P. *OSA Trends in Optics and Photonics: Advanced Solid-State Lasers*; Washington DC: Optical Society of America, 1999.
[55] Dergachev, A.; Wall, K.; Moulton, P. F. A CW side-pumped Tm: YLF laser. In *Proceedings of Advanced solid-state lasers*, Québec City Canada, 2002.
[56] So, S.; Mackenzie, J. I.; Shepherd, D. P.; Clarkson, W. A.; Betterton, J. G.; Gorton, E. K. A power-scaling strategy for longitudinally diode-pumped Tm:YLF lasers. *Appl. Phys. B* **2006**, *84*, 389–393.
[57] Ranieri, I. M.; Baldochi, S. L.; Santo, A. M. E.; Gomes, L.; Courrol, L. C.; Tarelho, L. V. G.; De Rossi, W.; Berretta, J. R.; Costa, F. E.; Nogueira, G. E. C. et al. Growth of $LiYF_4$ crystals doped with holmium, erbium and thulium. *J. Cryst. Growth* **1996**, *166*, 423–428.
[58] Ranieri, I. M.; Courrol, L. C.; Carvalho, A. F.; Gomes, L.; Baldochi, S. L. Growth of YLF:Yb:Tm:Nd for optical applications. *J. Mater. Sci.* **2007**, *42*, 2309–2313.
[59] Wyss, C.; Lüthy, W.; Weber, H. P.; Rogin, P.; Hulliger, J. Energy transfer in Yb^{3+}:Er^{3+}:YLF. *Opt. Commun.* **1997**, *144*, 31–35.
[60] Heumann, E.; Möbert, P.; Huber, G.; Chai, B. H. T. Room-temperature upconversion-pumped cw Yb, Er:$YLiF_4$ laser at 1.234 μm. In *Proceedings of Advanced Solid State Lasers*, San Francisco, California United States, 1996.
[61] Heine, F.; Ostroumov, V.; Heumann, E.; Jensen, T.; Huber, G.; Chai, B. H. T. CW Yb, Tm:$LiYF_4$ Upconversion Laser at 650 nm, 800 nm, and 1,500 nm. In *Proceedings of Advanced Solid State Lasers*, Memphis, Tennessee United States, 1995, pp 77–79.
[62] Wang, J.; Wang, F.; Xu, J.; Wang, Y.; Liu, Y. S.; Chen, X. Y.; Chen, H. Y.; Liu, X. G. Lanthanide-doped $LiYF_4$ nanoparticles: Synthesis and multicolor upconversion tuning. *C. R. Chimie* **2010**, *13*, 731–736.
[63] Mahalingam, V.; Vetrone, F.; Naccache, R.; Speghini, A.; Capobianco, J. A. Colloidal Tm^{3+}/Yb^{3+}-doped $LiYF_4$ nanocrystals: Multiple luminescence spanning the UV to NIR regions via low-energy excitation. *Adv. Mater.* **2009**, *21*, 4025–4028.
[64] Chen, G. Y.; Ohulchanskyy, T. Y.; Kachynski, A.; Ågren, H.; Prasad, P. N. Intense visible and near-infrared upconversion photoluminescence in colloidal $LiYF_4$:Er^{3+} nanocrystals under excitation at 1,490 nm. *ACS Nano* **2011**, *5*, 4981–4986.
[65] Hong, A. R.; Kim, S. Y.; Cho, S. H.; Lee, K.; Jang, H. S. Facile synthesis of multicolor tunable ultrasmall $LiYF_4$:Yb,Tm,Er/$LiGdF_4$ core/shell upconversion nanophosphors with sub-10 nm size. *Dyes Pigm.* **2017**, *139*, 831–838.
[66] Meijer, M. S.; Rojas-Gutierrez, P. A.; Busko, D.; Howard, I. A.; Frenzel, F.; Würth, C.; Resch-Genger, U.; Richards, B. S.; Turshatov, A.; Capobianco, J. A. et al. Absolute upconversion quantum yields of blue-emitting LiYF4:Yb^{3+},Tm^{3+} upconverting nanoparticles. *Phys. Chem. Chem. Phys.* **2018**, *20*, 22556–22562.
[67] Meesaragandla, B.; Sarkar, D.; Adusumalli, V. N. K. B.; Mahalingam, V. Double bond terminated Ln^{3+}-doped $LiYF_4$ nanocrystals with strong single band NIR emission: Simple click chemistry route to make water dispersible nanocrystals with various functional groups. *New J. Chem.* **2016**, *40*, 3080–3085.
[68] Na, H.; Jeong, J. S.; Chang, H. J.; Kim, H. Y.; Woo, K.; Lim, K.; Mkhoyan, K. A.; Jang, H. S. Facile synthesis of intense green light emitting $LiGdF_4$:Yb,Er-based upconversion bipyramidal nanocrystals and their polymer composites. *Nanoscale* **2014**, *6*, 7461–7468.
[69] Shin, J.; Kyhm, J. H.; Hong, A. R.; Song, J. D.; Lee, K.; Ko, H.; Jang, H. S. Multicolor tunable upconversion luminescence from sensitized seed-mediated grown $LiGdF_4$:Yb,Tm-based core/triple-shell nanophosphors for transparent displays. *Chem. Mater.* **2018**, *30*, 8457–8464.
[70] Park, B. J.; Hong, A. R.; Park, S.; Kyung, K. U.; Lee, K.; Seong Jang, H. Flexible transparent displays based on core/shell upconversion nanophosphor-incorporated polymer waveguides. *Sci. Rep.* **2017**, *7*, 45659.
[71] Zhang, Q.; Yan, B. Hydrothermal synthesis and characterization of $LiREF_4$ (RE = Y, Tb-Lu) nanocrystals and their core-shell nanostructures. *Inorg. Chem.* **2010**, *49*, 6834–6839.
[72] Xue, X. J.; Uechi, S.; Tiwari, R. N.; Duan, Z. C.; Liao, M. S.; Yoshimura, M.; Suzuki, T.; Ohishi, Y. Size-dependent upconversion luminescence and quenching mechanism of $LiYF_4$: Er^{3+}/Yb^{3+} nanocrystals with oleate ligand adsorbed. *Opt. Mater. Express* **2013**, *3*, 989–999.
[73] Dong, J.; Zhang, J.; Han, Q. Y.; Zhao, X.; Yan, X. W.; Liu, J. H.; Ge, H. B.; Gao, W. Tuning and enhancing the red upconversion emission of Er^{3+} in $LiYF_4$ nanoparticles. *J. Lumin.* **2019**, *207*, 361–368.
[74] Kim, S. Y.; Jeong, J. S.; Mkhoyan, K. A.; Jang, H. S. Direct observation of the core/double-shell architecture of intense dual-mode luminescent tetragonal bipyramidal nanophosphors. *Nanoscale* **2016**, *8*, 10049–10058.
[75] Liu, S. S.; Guo, X. Y.; Zhai, X. S.; Zhao, D.; Zheng, K. Z.; Qin, G. S.; Qin, W. P. Oleic acid-modified $LiYF_4$:Er,Yb nanocrystals for potential optical-amplification applications. *J. Nanosci. Nanotechnol.* **2014**, *14*, 3718–3721.
[76] Kim, S. Y.; Won, Y. H.; Jang, H. S. A strategy to enhance Eu^{3+} emission from $LiYF_4$:Eu nanophosphors and green-to-orange multicolor tunable, transparent nanophosphor-polymer composites. *Sci. Rep.* **2015**, *5*, 7866.
[77] Liu, J.; Rijckaert, H.; Zeng, M.; Haustraete, K.; Laforce, B.; Vincze, L.; Van Driessche, I.; Kaczmarek, A. M.; Van Deun, R. Simultaneously excited downshifting/upconversion luminescence from lanthanide-doped core/shell fluoride nanoparticles for multimode anticounterfeiting. *Adv. Funct. Mater.* **2018**, *28*, 1707365.
[78] Zhu, Y. R.; Zhao, S. W.; Zhou, B.; Zhu, H.; Wang, Y. F. Enhancing upconversion luminescence of $LiYF_4$:Yb,Er nanocrystals by Cd^{2+} doping and core–shell structure. *J. Phys. Chem. C* **2017**, *121*, 18909–18916.
[79] Cheng, T.; Ortiz, R. F.; Vedantham, K.; Naccache, R.; Vetrone, F.; Marks, R. S.; Steele, T. W. J. Tunable chemical release from polyester thin film by photocatalytic zinc oxide and doped $LiYF_4$ upconverting nanoparticles. *Biomacromolecules* **2015**, *16*, 364–373.
[80] Jalani, G.; Naccache, R.; Rosenzweig, D. H.; Lerouge, S.; Haglund, L.; Vetrone, F.; Cerruti, M. Real-time, non-invasive monitoring of hydrogel degradation using LiYF4:Yb^{3+}/Tm^{3+} NIR-to-NIR upconverting nanoparticles. *Nanoscale* **2015**, *7*, 11255–11262.

[81] Cheng, T.; Marin, R.; Skripka, A.; Vetrone, F. Small and bright lithium-based upconverting nanoparticles. *J. Am. Chem. Soc.* **2018**, *140*, 12890–12899.

[82] Rojas-Gutierrez, P. A.; DeWolf, C.; Capobianco, J. A. Formation of a supported lipid bilayer on faceted $LiYF^4$:Tm^{3+}/Yb^{3+} upconversion nanoparticles. *Part. Part. Syst. Charact.* **2016**, *33*, 865–870.

[83] Yu, Q.; Rodriguez, E. M.; Naccache, R.; Forgione, P.; Lamoureux, G.; Sanz-Rodriguez, F.; Scheglmann, D.; Capobianco, J. A. Chemical modification of temoporfin-a second generation photosensitizer activated using upconverting nanoparticles for singlet oxygen generation. *Chem. Commun.* **2014**, *50*, 12150–12153.

[84] Mahalingam, V.; Naccache, R.; Vetrone, F.; Capobianco, J. A. Sensitized Ce^{3+} and Gd^{3+} ultraviolet emissions by Tm^{3+} in colloidal $LiYF_4$ nanocrystals. *Chem.—Eur. J.* **2009**, *15*, 9660–9663.

[85] Mahalingam, V.; Naccache, R.; Vetrone, F.; Capobianco, J. A. Preferential suppression of high-energy upconverted emissions of Tm^{3+} by Dy^{3+} ions in Tm^{3+}/Dy^{3+}/Yb^{3+}-doped $LiYF_4$ colloidal nanocrystals. *Chem. Commun.* **2011**, *47*, 3481–3483.

[86] Chien, H. W.; Wu, C. H.; Yang, C. H.; Wang, T. L. Multiple doping effect of $LiYF_4$:Yb^{3+}/Er^{3+}/Ho^{3+}/Tm^{3+}@$LiYF_4$:Yb^{3+} core/shell nanoparticles and its application in Hg^{2+} sensing detection. *J. Alloys Compd.* **2019**, *806*, 272–282.

[87] Chung, Y. C.; Yang, C. H.; Lee, R. H.; Wang, T. L. Dual stimuli-responsive block copolymers for controlled release triggered by upconversion luminescence or temperature variation. *ACS Omega* **2019**, *4*, 3322–3328.

[88] Marin, R.; Labrador-Paéz, L.; Skripka, A.; Haro-González, P.; Benayas, A.; Canton, P.; Jaque, D.; Vetrone, F. Upconverting nanoparticle to quantum dot förster resonance energy transfer: Increasing the efficiency through donor design. *ACS Photonics* **2018**, *5*, 2261–2270.

[89] Möller, N.; Hellwig, T.; Stricker, L.; Engel, S.; Fallnich, C.; Ravoo, B. J. Near-infrared photoswitching of cyclodextrin-guest complexes using lanthanide-doped $LiYF_4$ upconversion nanoparticles. *Chem. Commun.* **2017**, *53*, 240–243.

[90] Homann, C.; Krukewitt, L.; Frenzel, F.; Grauel, B.; Würth, C.; Resch-Genger, U.; Haase, M. $NaYF_4$:Yb, Er/$NaYF_4$ core/shell nanocrystals with high upconversion luminescence quantum yield. *Angew. Chem., Int. Ed.* **2018**, *57*, 8765–8769.

[91] Mondini, S.; Ferretti, A. M.; Puglisi, A.; Ponti, A. Pebbles and PebbleJuggler: Software for accurate, unbiased, and fast measurement and analysis of nanoparticle morphology from transmission electron microscopy (TEM) micrographs. *Nanoscale* **2012**, *4*, 5356–5372.

[92] Rodriguez-Carvajal, J. *Introduction to the Program FullProf*; Laboratoire Léon Brillouin, France, 2003.

[93] Cui, X. P.; Feng, Z. J.; Jin, Y.; Cao, Y. M.; Deng, D. M.; Chu, H.; Cao, S. X.; Dong, C.; Zhang, J. C. *AutoFP*: A GUI for highly automated Rietveld refinement using an expert system algorithm based on *FullProf*. *J. Appl. Crystallogr.* **2015**, *48*, 1581–1586.

[94] Kaiser, M.; Würth, C.; Kraft, M.; Hyppänen, I.; Soukka, T.; Resch-Genger, U. Power-dependent upconversion quantum yield of $NaYF_4$:Yb^{3+},Er^{3+} nano- and micrometer-sized particles-measurements and simulations. *Nanoscale* **2017**, *9*, 10051–10058.

[95] Rinkel, T.; Raj, A. N.; Dühnen, S.; Haase, M. Synthesis of 10 nm β-$NaYF_4$:Yb,Er/$NaYF_4$ core/shell upconversion nanocrystals with 5 nm particle cores. *Angew. Chem., Int. Ed.* **2016**, *55*, 1164–1167.

[96] Arppe, R.; Hyppänen, I.; Perälä, N.; Peltomaa, R.; Kaiser, M.; Würth, C.; Christ, S.; Resch-Genger, U.; Schäferling, M.; Soukka, T. Quenching of the upconversion luminescence of $NaYF_4$:Yb^{3+},Er^{3+} and $NaYF_4$:Yb^{3+},Tm^{3+} nanophosphors by water: The role of the sensitizer Yb^{3+} in non-radiative relaxation. *Nanoscale* **2015**, *7*, 11746–11757.

[97] Würth, C.; Fischer, S.; Grauel, B.; Alivisatos, A. P.; Resch-Genger, U. Quantum yields, surface quenching, and passivation efficiency for ultrasmall core/shell upconverting nanoparticles. *J. Am. Chem. Soc.* **2018**, *140*, 4922–4928.

[98] Dos Santos, M. A. C.; Antic-Fidancev, E.; Gesland, J. Y.; Krupa, J. C.; Lemaître-Blaise, M.; Porcher, P. Absorption and fluorescence of Er^{3+}-doped $LiYF_4$: Measurements and simulation. *J. Alloys Compd.* **1998**, *275–277*, 435–441.

[99] Bensalah, A.; Guyot, Y.; Ito, M.; Brenier, A.; Sato, H.; Fukuda, T.; Boulon, G. Growth of Yb^{3+}-doped $YLiF_4$ laser crystal by the Czochralski method. Attempt of Yb^{3+} energy level assignment and estimation of the laser potentiality. *Opt. Mater.* **2004**, *26*, 375–383.

[100] Garcia, E.; Ryan, R. R. Structure of the laser host material $LiYF_4$. *Acta Crystallogr. Sec. C* **1993**, *49*, 2053–2054.

[101] Thoma, R. E.; Weaver, C. F.; Friedman, H. A.; Insley, H.; Harris, L. A.; Yakel, H. A. Jr. Phase equilibria in the system LiF—YF_3. *J. Phys. Chem.* **1961**, *65*, 1096–1099.

[102] Spinger, B.; Danilov, V. P.; Prokhorov, A. M.; Schwan, L. O.; Schmid, D. Up conversion processes in yttrium-lithium-flouride crystals co-doped with erbium and ytterbium ions. In *Proceedings of XI Feofilov Symposium on Spectroscopy of Crystals Activated by Rare-Earth and Transition Metal Ions*, Kazan, Russian Federation, 2002, pp 191–203.

[103] Chen, X.; Xu, W.; Song, H. W.; Chen, C.; Xia, H. P.; Zhu, Y. S.; Zhou, D. L.; Cui, S. B.; Dai, Q. L.; Zhang, J. Z. Highly efficient $LiYF_4$:Yb^{3+}, Er^{3+} upconversion single crystal under solar cell spectrum excitation and photovoltaic application. *ACS Appl. Mater. Interfaces* **2016**, *8*, 9071–9079.

[104] Saleta Reig, D.; Grauel, B.; Konyushkin, V. A.; Nakladov, A. N.; Fedorov, P. P.; Busko, D.; Howard, I. A.; Richards, B. S.; Resch-Genger, U.; Kuznetsov, S. V. et al. Upconversion properties of SrF_2:Yb^{3+},Er^{3+} single crystals. *J. Mater. Chem. C* **2020**, *8*, 4093–4101.